Int. J. Electrochem. Sci., 14 **(2019)** 9948 – 9959, doi: 10.20964/2019.10.50

International Journal of ELECTROCHEMICAL SCIENCE
www.electrochemsci.org

Investigation of Influence of Microstructure on FH32 Steel Corrosion Properties using Gleeble Simulation of Heat-Affected Zone and Electrochemical Methods

Zuo-peng Zhao [1], *Peng-fei Xu* [1,*], *Hong-xia Cheng* [1], *Xiang-yu Lu* [1], *Jili Miao* [2], *Yunsai Chen* [3], *Lei Yang* [3]

[1] College of Harbor Coastal and Offshore Engineering, Hohai University, Nanjing 210098, China
[2] Jiangnan Shipyard (Group) Co. LTD., Shanghai 201913, China
[3] National Deep Sea Center, Qingdao 266237, China.
[*]E-mail: xupengfei@hhu.edu.cn

Received: 15 June 2019 / *Accepted:* 30 July 2019 / *Published:* 30 August 2019

The corrosion behavior was investigated for each heat-affected zone (HAZ) comprising a FH32 steel immersed in 3.5% NaCl solutions. To research the corrosion behavior of each HAZ sub-region, HAZ thermo-mechanical simulations were performed prior to the electrochemical tests. The results revealed that the corrosion resistance of the fine-grained HAZ (FGHAZ) comprising the steel is superior to that of other HAZ sub-regions. Moreover, the coarse-grained HAZ (CGHAZ) exhibited the worst corrosion resistance of the weld joint. The changes in the corrosion resistance of the HAZ sub-regions were attributed to variations in the microstructural sensitivity to corrosion behavior. Furthermore, the results indicated that the number, size, and distribution of martensite/austenite (M/A) constituents, as well as the grain size of the relevant phase can affect the resistance.

Keywords: C-Mn steel; heat-affected zone; EIS; microstructure; corrosion behavior

1. INTRODUCTION

Due to their favorable low-temperature properties, C-Mn steels have been used increasingly in building special ships (including liquefied natural gas (LNG) ships, liquefied petroleum gas (LPG) ships, and icebreakers) all over the world [1–2]. The requirements of ship steels include high strength, low-temperature toughness, and excellent corrosion resistance to the seawater during prolonged exposure to harsh ocean environments [3–4]. Several studies have shown that this resistance is affected by the microstructure of the steel [4–5].

Welding is the most commonly used method for ship structure connections. However, microstructural evolution will occur in and around the welded area during the welding process, leading to performance deterioration of the welded joints [6–7]. From a metallurgical point of view, welding can be identified as a thermal cycle that consists of continuous heating to a certain peak temperature and cooling to room temperature [8]. The weld thermal cycle changes the base metal (BM), thereby resulting in an inhomogeneous microstructure in the heat-affected zone (HAZ) [9]. According to previous studies, the HAZ is typically the most susceptible to potential corrosion failures, and these failures are closely correlated with the HAZ microstructures [4–5, 10–11]. The evaluation and prediction of corrosion behavior are essential for avoiding catastrophic failure particularly in welded structures [12]. Hence, a study of the HAZ corrosion properties is warranted.

Previous studies considering the effect of HAZ microstructure on corrosion behavior have focused mainly on welded joint specimens [4, 13–14]. However, research of the HAZ in actual welded joints is difficult due to the narrowness of the HAZ [15]. As a suitable method of preparing specimens, welding thermal simulation has been used to investigate and identify the various HAZ sub-regions [16–17]. Hutchinson et al. revealed, via simulations, the relationships between HAZ microstructures and toughness [18]. Mohammadi et al. investigated the effect of the post welding microstructure on the corrosion behavior of HAZ comprising API X-80 pipeline steel [17].

In this work, experiments have been conducted on an industrial FH32 grade steel. The corrosion behavior of each HAZ sub-region was investigated by first performing HAZ thermo-mechanical simulations. Electrochemical tests were then performed on the simulated HAZ by exposing each to 3.5% NaCl solutions. The effects of each HAZ sub-region microstructure on the corrosion behavior were investigated.

2. MATERIALS AND EXPERIMENTAL PROCEDURE

2.1 Materials

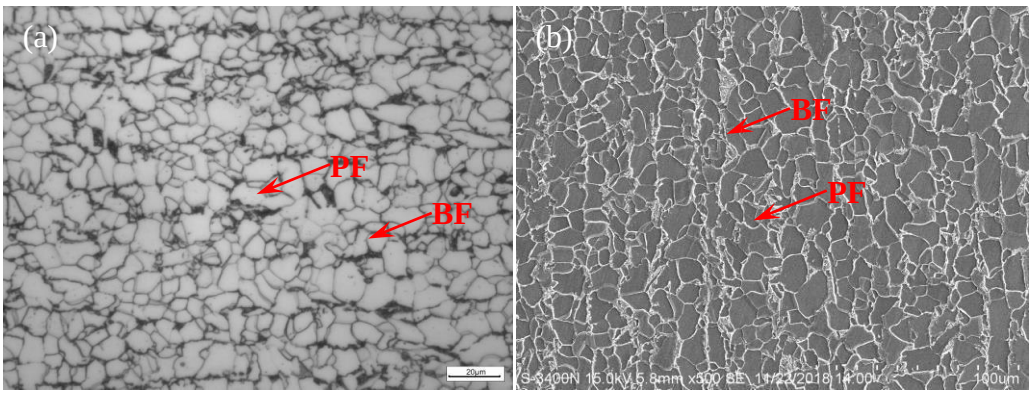

Figure 1. OM and SEM micrographs of BM.

Table 1. Chemical composition (in wt%) of FH32 steel selected in the present study.

C	Mn	Si	P	S	Mo	Ni	Cr	Cu	Nb	Ti	Al
0.096	1.44	0.22	0.009	0.002	0.006	0.001	0.042	0.01	0.005	0.011	0.055

In this work, stiffened plates (thickness: 15 mm) of an industrial FH32 grade steel were investigated (see **Table 1** and **Figure 1** for the chemical composition and micrographs of the material). The steel was composed of an as-rolled mixed microstructure of polygonal ferrite (PF) and bainite (BF).

Thermal cycling simulations typical of the HAZ thermal cycles (heat input: 45 kJ/cm, consistent with practical production) were performed on 10 × 10 × 65 mm samples in a thermomechanical Gleeble-3800 system. **Figure 2** shows the thermal cycle procedure based on ANSYS analysis. For example, the specimen obtained from the coarse-grained heat affected zone (CGHAZ) was heated at a rate of 130 °C/s to a peak temperature of 1350 °C and held for 1 s. The specimen was then cooled to 800 °C in 24 s and to 500 °C in 54 s. The other thermal cycles were performed at different peak temperatures, and the cooling speeds from 800 °C to 200 °C were the same as those employed for the aforementioned thermal cycle.

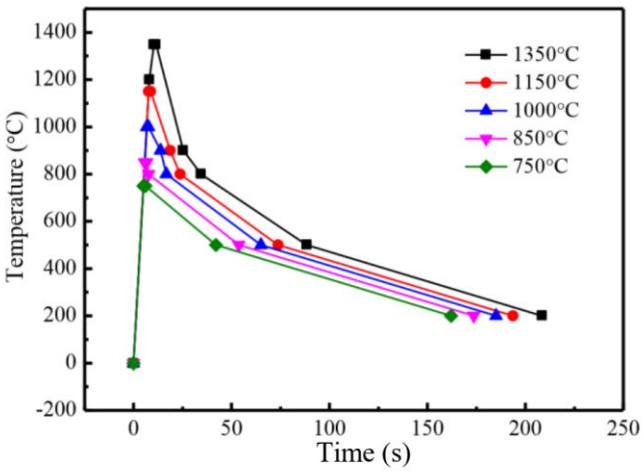

Figure 2. The thermal cycle procedure for the experiments.

After the HAZ thermo-mechanical simulations, electrochemical tests were performed on the samples that were machined from the HAZ samples, as shown in **Figure 3**. These tests were conducted in the HAZ simulation zones.

2.2 Experimental procedure

Electrochemical tests, including potentiodynamic polarization measurements and electrochemical impedance spectroscopy (EIS), were used to evaluate the corrosion properties of HAZ comprising the FH32 steel immersed in 3.5% NaCl solutions at room temperature. The electrochemical

tests were performed using a CS350 electrochemical workstation (Corrtest Instruments, China). A three-electrode glass corrosion cell was employed with a platinum electrode and a saturated calomel electrode (SCE) as the counter electrode and the reference electrode, respectively. The HAZ simulated specimens, as the working electrode, were immersed in the NaCl solutions for 30 min. Prior to the EIS tests, the open circuit potential (OCP) of the simulated HAZ samples was measured for at least 30 min. The corresponding potentidynamic polarization plots were recorded at a scan rate of 1 mV/s at the OCP to determine the corrosion current density (I_{corr}) and the corrosion potentials (E_{corr}). Each experiment was performed in triplicate.

The analysis of microstructures was performed using optical microscopy (OM), scanning electron microscopy (SEM), and electron back-scattered diffraction (EBSD). The SEM (S-3400N) and EBSD (EDAX) were used to observe microstructure evolution.

The microstructures were characterized via optical microscopy (OM), scanning electron microscopy (SEM; S-3400N), and electron back-scatter diffraction (EBSD; EDAX). Similarly, the corresponding microstructural evolution was characterized via SEM and EBSD.

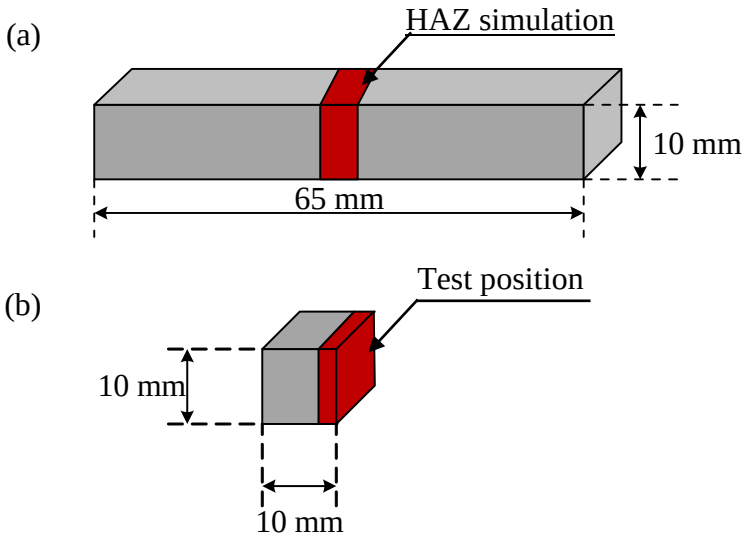

Figure 3. Geometry of (a) the thermal cycling simulations test and (b) the electrochemical test specimens.

3. RESULTS

3.1 Microstructure changes in HAZ

Figure 4 shows OM images of the simulated welded microstructures of the FH32 steel at different peak temperatures. The CGHAZ (1350 °C) microstructure consists of granular bainite (GB) and the prior austenite grain boundary network [**Fig. 4(a)**]. GB is manifested as island constituents distributed in the matrix. These constituents, which are typically referred to as martensite/austenite (M/A) constituents, are transformed from retained austenite during accelerated cooling processes [19]. Owing to excessive heating at high temperatures, the prior austenite grain size increases significantly.

As the peak temperature decreases to 1150 °C, the microstructure consists mainly of quasi-polygonal ferrite (QF) and BF and the prior austenite grain boundaries disappear. This region is referred to as the fine-grained heat affected zone (FGHAZ) [**Fig. 4(b)**]. When the peak temperature decreases to 1000 °C, the microstructures are further refined [**Fig. 4(c)**]. The resulting intercritical-grained heat affected zone (ICHAZ) (850–750 °C), i.e., an as-rolled mixed microstructure of PF and BF [**Fig. 4(d) and (e)**], is similar to the BM.

3.2 Impedance Measurements

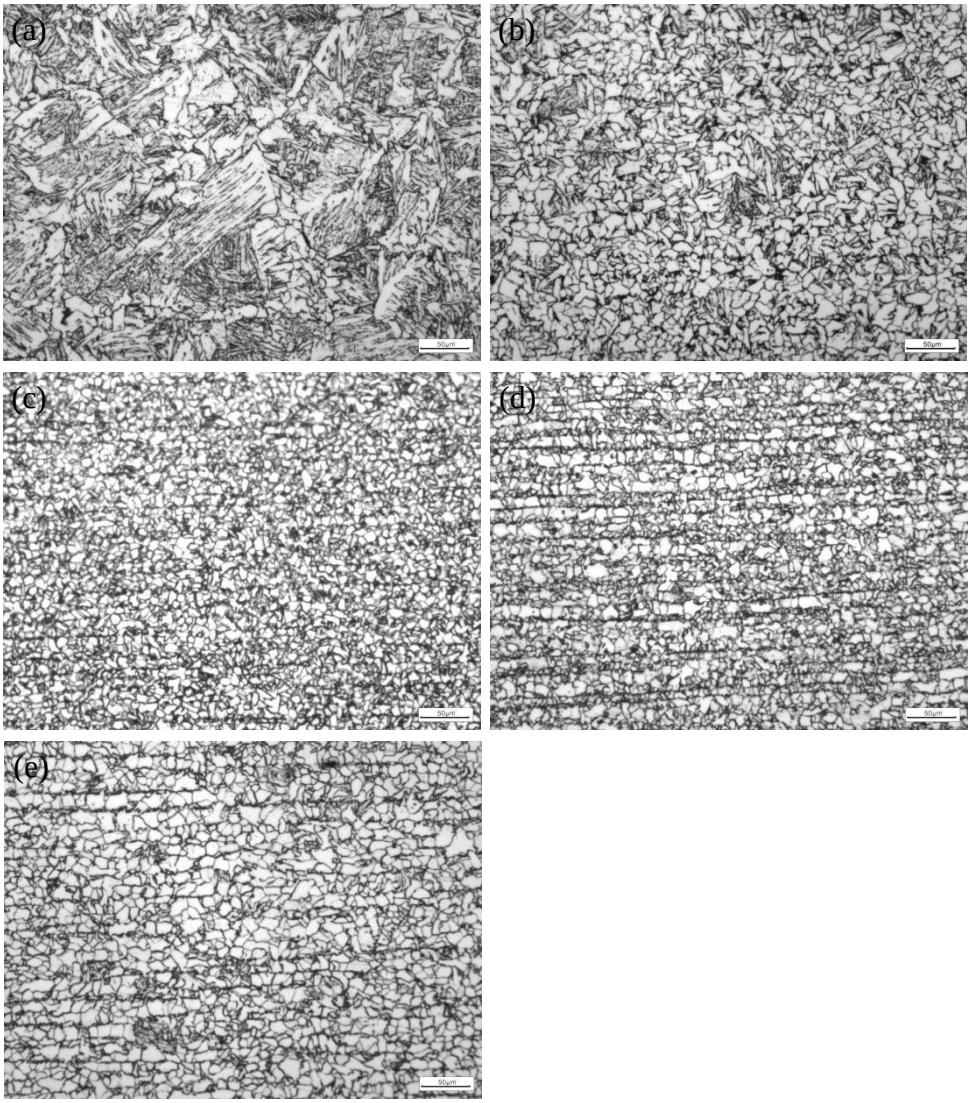

Figure 4. OM images of the simulated welded microstructures (a) 1350 ℃, (b) 1150 ℃, (c) 1000 ℃, (d) 850 ℃ and (e) 750 ℃.

As a powerful and non-destructive electrochemical technique, EIS can be used for accurate investigation of the interface reaction ability at the metal/film interface and the formation of corrosion products [1,20]. **Figure 5** shows impedance spectra obtained for the simulated welded microstructures of FH32 steel at different peak temperatures. In the Nyquist plots [**Fig. 5(a)**], the maximum and minimum impedance-loop diameters are realized at peak temperatures of 1000 ℃ and 1350 ℃,

respectively. The diameters of the impedance arcs associated with BM are very similar to those associated with peak temperatures of 1150 °C, 850 °C, and 750 °C. Peak temperatures of 1350 °C, 1000 °C, and 850 °C correspond to CGHAZ, FGHAZ, and ICHAZ, respectively. Thus, compared with the rates of other sub-regions, the corrosion rates are considerably lower in FGHAZ and higher in CGHAZ. This may have resulted from the effect of microstructure on the corrosion behavior. The Bode plots indicate that, like the impedance dependence on the frequency, the phase-angle dependence on the frequency is the same, regardless of the peak temperature [**Fig. 5(b)**]. Only one peak maximum appeared in the low-frequency range, suggesting that the characteristic phase maxima yield only one time constant for the HAZ sub-regions of FH32 steel.

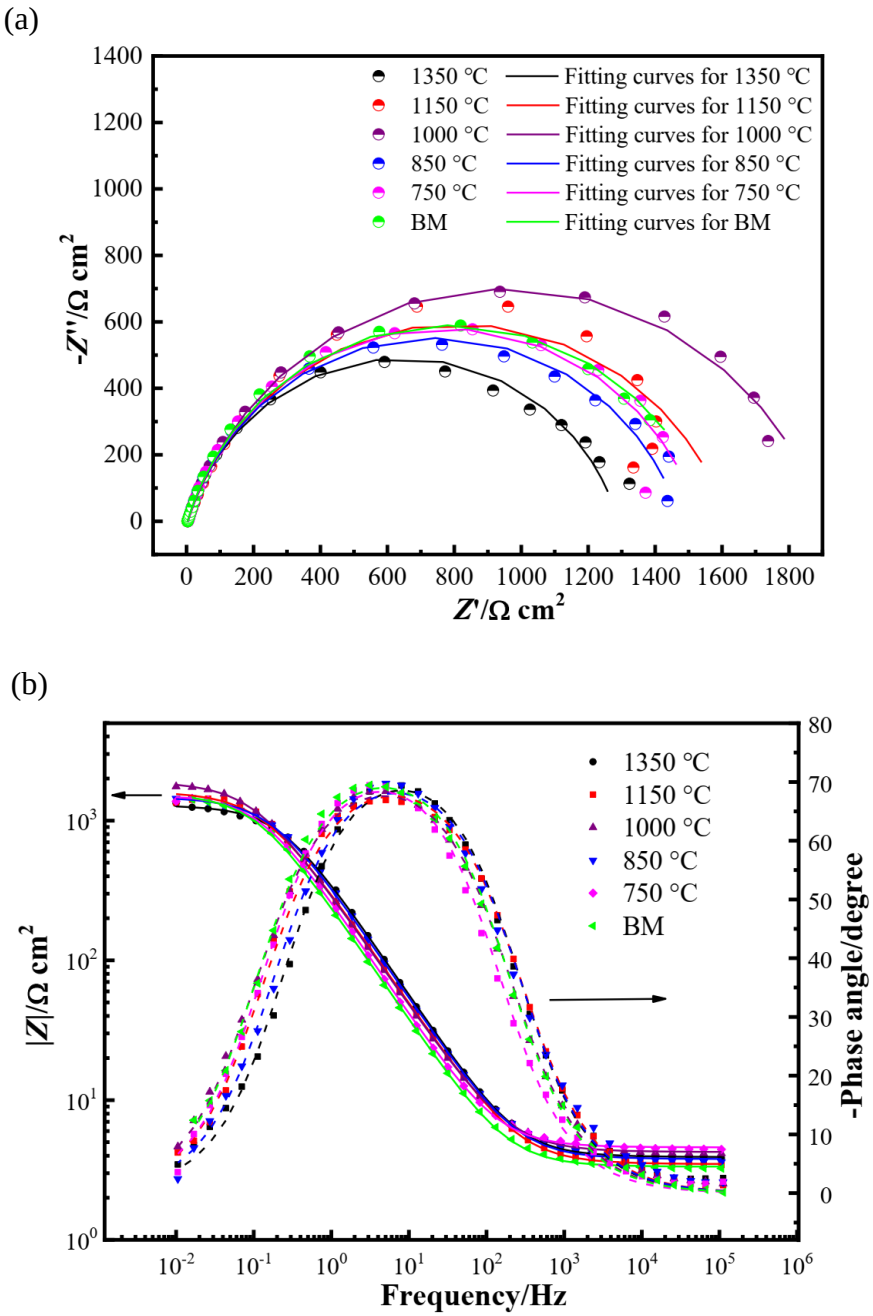

Figure 5. Impedance spectra of BM and simulated welded microstructures at different peak temperatures in NaCl solution, (a) Nyquist plots, and (b) Bode plots.

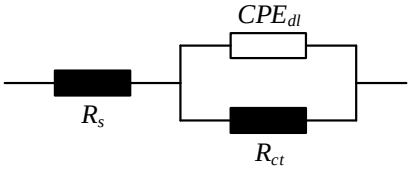

Figure 6. Equivalent electrical circuits used to fit EIS spectra.

Using the Zsimpwin software [22–23], the EIS results are further analyzed by an equivalent circuit (**Fig. 6**). As shown in **Fig. 5**, the experimental data are well-fitted by the circuit. Each equivalent circuit is characterized by R_s the solution resistance, CPE_{dl} the double-layer capacitance at the surface of the electrolyte solution and the steel substrate, and R_{ct} the charge transfer resistance. The impedance of CPE is given as follows:

$$Z_{CPE} = Y_0 \cdot [(j\omega)^n]^{-1} \quad (1)$$

Where, Z_{CPE}, Y_0, ω, and α are the impedance of the CPE, CPE constant, frequency (Hz), and phase angle of the CPE (radians), respectively, and the exponent n is equal to α/(α/2). **Table 2** lists the fitting parameters of the BM and simulated welded microstructures at different peak temperatures. The maximum R_{ct} occurs at a peak temperature of 1000 °C, indicating that FGHAZ exhibits greater corrosion resistance than the other HAZ sub-regions.

Table 2. Fitting parameters of EIS measurements of BM and simulated welded microstructures at different peak temperatures.

Peak temperature (°C)	CPE_{dl} ($\Omega^{-1}s^n cm^{-2}$)	n	R_{ct} (Ω)
1350	5.752E-4	0.829	1286
1150	7.247E-4	0.807	1614
1000	7.478E-4	0.809	1898
850	6.334E-4	0.819	1473
750	8.070E-4	0.826	1529
BM	8.918E-4	0.823	1529

3.3 Potentiodynamic polarization tests

The corrosion behavior of the simulated welded microstructures at different peak temperatures was further investigated via potentiodynamic polarization tests (see **Figure 7** and **Table 3** for the obtained potentidynamic polarization curves and corresponding data). The corrosion characteristics of the FH32 steel vary with the peak temperature conditions. For example, the corrosion potential (E_{corr}) value and corrosion current density (I_{corr}) are maximum and minimum, respectively, at a peak temperature of 1000 °C. Conversely, the maximum I_{corr} occurs at a peak temperature of 1350 °C. These results indicate that the corrosion resistance of FGHAZ is better than that of other HAZ sub-regions, and CGHAZ exhibits the worst corrosion resistance in the weld joint, consistent with the previously obtained EIS results.

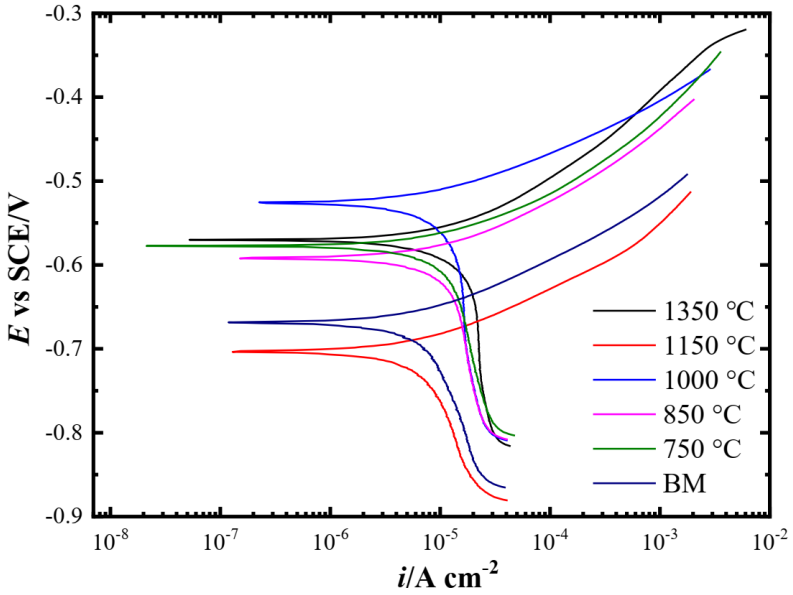

Figure 7. Potentidynamic polarization curves of BM and simulated welded microstructures at different peak temperatures in NaCl solution.

Table 3 Fitting parameters of Tafel curves of base metal and simulated welded microstructures at different peak temperatures.

Peak temperature (°C)	β_a (mV·dec^{-1})	β_c (mV·dec^{-1})	E_{corr} (V)	I_{corr} (μA·cm^{-2})
1350	105	1.13E+07	-0.570	25.05
1150	70	516	-0.703	8.89
1000	64	1180	-0.526	1.29
850	84	3753	-0.592	17.78
750	93	4402	-0.577	18.30
BM	71	526	-0.669	9.34

4. DISCUSSION

The impedance measurements and potentiodynamic polarization tests reveal considerable differences in the corrosion behaviors of the different HAZ sub-regions. Compared with the alloying-element content of the micro-alloy steel, the microstructure plays a dominant role in corrosion behavior [23], i.e., this behavior is related to changes in the microstructural sensitivity of corrosion behavior.

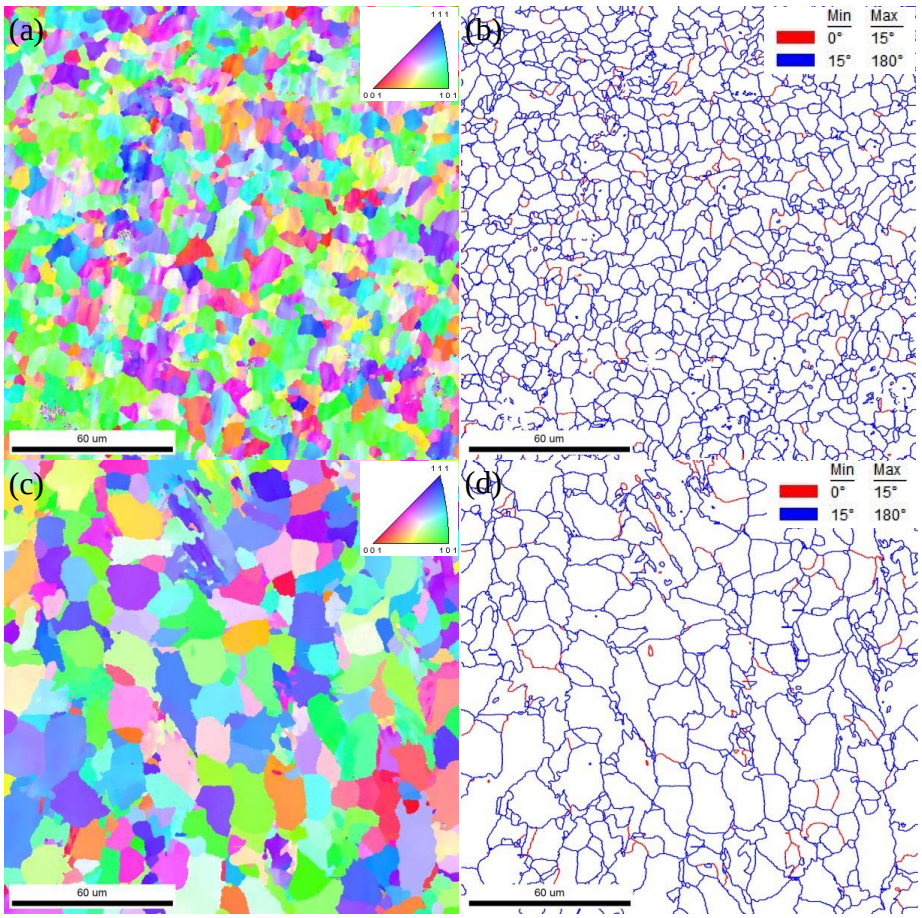

Figure 8. Crystallographic characteristics of FGHAZ and BM. (a) and (c) orientation image maps, (b) and (d) image quality maps with grain boundary misorientation distribution.

The EIS results show that the corrosion rates decrease significantly in FGHAZ (**Fig. 5)**, due (as previously mentioned) to the refined grain size. During the weld thermal cycle, the FGHAZ undergoes full austenitization, but the austenite grains undergo incomplete growth. Austenite is transformed into bainite during the subsequent cooling process and, owing to recrystallization, the grains in FGHAZ are further refined. **Figure 8** shows the orientation image maps and the corresponding image quality maps with grain boundary misorientation distribution of FGHAZ and BM. The average grain size of FGHAZ is significantly smaller than that of BM. Previous studies indicate that the refined grain size plays a positive role in the corrosion behavior, including inducing improvements in the intergranular and pitting corrosion resistance [24–25]. Furthermore, the uniform fine grains are accompanied by a large number of low angle boundaries in FGHAZ, and these boundaries are effective in arresting the intergranular corrosion [24]. Therefore, the corrosion rates in FCHAZ are lower than those of other HAZ sub-regions.

The corrosion resistance of specimens at a peak temperature of 850 °C is weaker than that of the specimens at a peak temperature of 1000 °C, although the specimens have approximately the same grain size (**Fig. 4)**. This results from the differing corrosion behavior of different phases. As shown in **Fig. 9(c)**, the microstructure consists of an as-rolled PF/BF mixed microstructure, with many M/A constituents (as the secondary phase) occurring in the BF. The microstructure and chemical components

of these constituents differ (to some extent) from those of the matrix, leading possibly to the galvanic effect. Present studies indicate that, compared with other phases, the M/A constituents are more negative in the galvanic potential series, owing to the strain energy associated with these components [25]. Thus, the large number of these constituents in the BF lead to a poor corrosion resistance. In contrast, for the specimens at a peak temperature of 1000 °C, the M/A constituents in BM undergo significant decomposition due to the full austenitization. The accompanying precipitation of numerous carbide particles provides favorable conditions for recrystallization. Consequently, the granular and fine M/A constituents are uniformly distributed in the matrix [**Fig. 9(b)**], thereby yielding a weak galvanic effect.

In CGHAZ, the microstructure is mainly composed of GB, a small amount of BF, and many bulk M/A constituents distributed in the matrix [**Fig. 9(c)**]. The corrosion resistance decreases significantly, owing to these relatively coarse M/A constituents [5]. The resistance also decreases due to the GB, a nonequilibrium microstructural feature, which induces a high welding residual stress and dislocation density. Therefore, the corrosion resistance of CGHAZ is lower than that of other HAZ sub-regions (**Tables 2** and **3**).

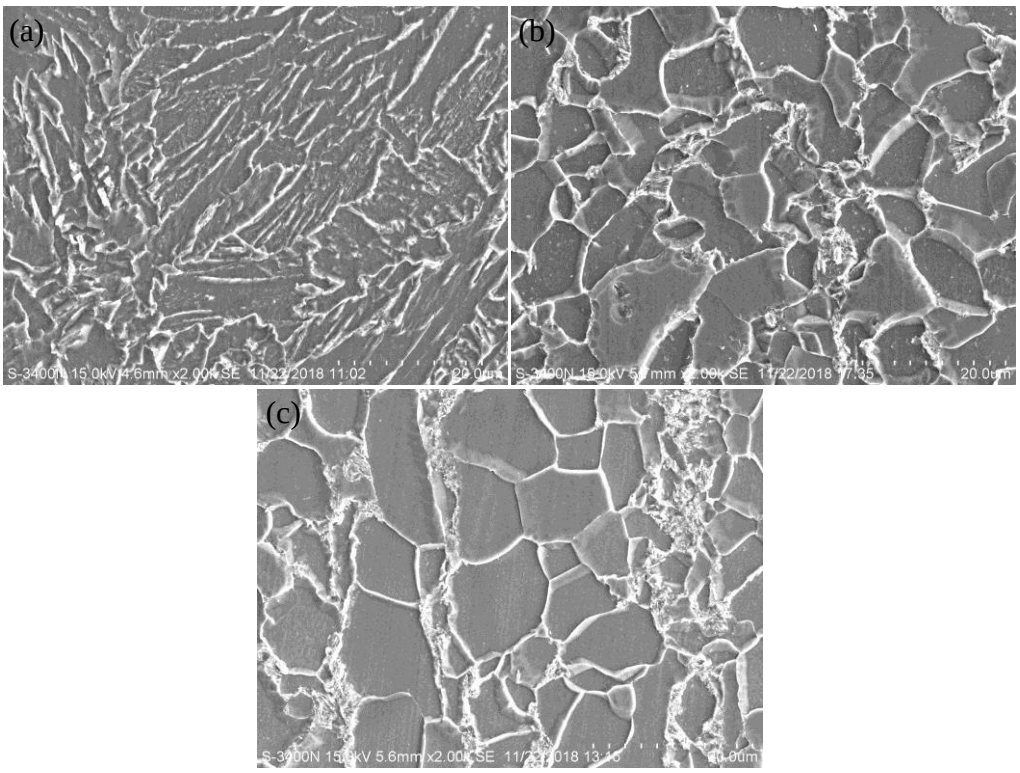

Figure 9. SEM micrographs showing the microstructures at different peak temperature, (a) 1350 ℃, (b) 1000 ℃and (c) 850 ℃.

5. CONCLUSIONS

In this work, the corrosion behavior characterizing simulated HAZ specimens of FH32 steel in 3.5% NaCl solutions was investigated. The main conclusions of the study are summarized as follows:

(1) Changes in the corrosion resistance of the sub-regions are attributed to variations in the microstructural sensitivity to corrosion behavior. This resistance can be affected by the number, size, and distribution of M/A constituents, as well as the grain size of the material.

(2) In 3.5% NaCl solutions, the corrosion resistance of the FGHAZ comprising the material is superior to that of other HAZ sub-regions. This is attributed to the refined grain size, as well as granular and fine M/A constituents of the microstructure. CGHAZ exhibits the worst corrosion resistance in the weld joint, due to severe coarsening of these constituents and a high welding residual stress.

ACKNOWLEDGEMENTS
This work was financially supported by the Fundamental Research funds for the Central Universities (No. 2018B13214), the Natural Science Foundation of China (No. 51609078), and the Natural Science Foundation of Jiangsu Province (No. BK20160875).

References

1. H.D. Li, Y.H. Dong, Y.Y. Shen, *International Journal of Electrochemical Science*, 12 (2017) 11077.
2. Y.Y. Shen, Y.H. Dong, H.D. Li, X.T. Chang, D.S. Wang, Q.H. Li and Y.S. Yin, *International Journal of Electrochemical Science*, 13 (2018) 6310.
3. Z.X. Wang, J.H. Zhao, J.G. Fang, X.H Jia, B. Zhang and G.Q. Ding, *Journal of Iron and Steel Research International*, 20 (2013) 85.
4. Y.P. Wang, X.R. Zuo and J.L. Li, *Steel Research International*, 86 (2015) 1260.
5. W. Zhao, Y. Zou, K.J. Matsuda and Z.D. Zou, *Materials and Design*, 99 (2016) 44.
6. Y.H. Yang, L. Shi, Z. Xu, H.S. Lu, X. Chen and X. Wang, *Engineering Fracture Mechanics*, 118 (2015) 337.
7. S. Kim, D. Kang, T.W. Kim, J. Lee and C. Lee, *Materials Science and Engineering A*, 528 (2011) 2331.
8. M. Zhao, F. Wei, W.Q. Huang and Y. Lei, *Science and Technology of Welding and Joining*, 20 (2015) 622.
9. M.P. Singh, R. Kumar, D.K. Shukla and K.S. Arora, *Materials Research Express*, 6 (2019) 1.
10. X.F. Yang and J.E. Castle, *Surface and Interface Analysis*, 33 (2002) 894.
11. L.W. Wang, Z.Y. Liu, Z.Y. Cui, C.W. Du, X.H. Wang and X.G. Li, *Corrosion Science*, 85 (2014) 401.
12. J.S. Mandke, *Oil Gas Journal*, 10 (1990) 40.
13. B. Jegdic, B. Bobic, B. Radojkovic, B. Alic and L. Radovanovic, *Journal of Materials Processing Technology*, 266 (2019) 579.
14. K. Qi, R.F. Li, G.J. Wang, G.Z. Li, B. Liu and M.F. Wu, *Journal of Materials Engineering and Performance*, 28 (2019) 287.
15. Z. Boumerzoug, E. Raouache and F. Delaunois, *Materials Science and Engineering A*, 530 (2011) 191.
16. Y. Ci and Z.Z. Zhang, *Journal of Iron and Steel Research, International*, 21 (2017) 966.
17. F. Mohammadi, F.F. Eliyan and A. Alfantazi, *Corrosion Science*, 63 (2012) 323.
18. B. Hutchinson, J. Komenda, G.S. Rohrer and H. Beladi, *Acta Materialia*, 97 (2015) 380.
19. X.W. Chen, G.Y. Qiao, X.L. Han, X. Wang, F.R. Xiao and B. Liao, *Materials and Design*, 53 (2014) 888.
20. X.G. Feng, X.Y. Lu, Y. Zuo, N. Zhuang and D. Chen, *Corrosion Science*, 103 (2016) 223.

21. H. Gerengi, P. Slepski and G. Bereket, *Materials And Corrosion*, 64 (2013) 1024.
22. N. Wei, Y. Jiang, Y. Ying, X. Guo, Y. Wu, Y. Wen and H. Yang, *RSC Advances*, 7 (2017) 11528.
23. S. Maitra and G.C. English, *Metallurgical Transactions A*, 12 (1981) 535.
24. Z.F. Wang, P.H. Li, Y. Guan, Q.F. Chen and S.K. Pu, *Corrosion Science*, 51 (2009) 954.
25. A.S. Hamada, L.P. Karjalainen and M.C. Somani, *Materials Science and Engineering A*, 431 (2006) 211.